**ORIGINAL CONTRIBUTION**

# Evolution of morphology and morphology stability in PP/PA6/EPDM-g-MA reactive ternary blends using viscoelastic measurements

Bahareh Afsari[1,2] · Mir Karim Razavi Aghjeh[1,2] · Maryam Hasanpour[1,2]

## Abstract

The relationship between the morphology and rheological properties of PP/PA6/EPDM-g-MA ternary blends, at relatively low rubber phase contents, was studied in detail. The results showed that the size of composite droplets of core-shell microstructures decreased and increased after passing through a minimum due to competitive effects of the emulsification role of EPDM-g-MA and viscosity ratio. This trend in morphology development was well reflected in the relaxation spectrums of the blends. The morphology of discrete core-shell particles altered to the large clusters of core-shell particles at higher rubbery phase contents which led to alteration of viscoelastic behavior from liquid-like to solid-like. The morphology of high EPDM-g-MA content ternary blends was unstable particularly at higher temperatures which was evaluated using time-sweep rheological experiments and confirmed via direct SEM analysis.

**Keywords** Ternary blend · Compatibilization · Rheology · Morphology · Shape relaxation

## Introduction

Melt mixing of two or more polymers is a common way widely used in the industry to obtain new high-performance materials without the expense of synthesizing new polymers (Han 1981; Horiuchi et al. 1997; Utracki and Wilkie 2002; Kim et al. 2004; Wilkinson et al. 2004; Yin et al. 2007). The morphology of immiscible polymer pairs (polymer blends) is strongly dependent on the fractions, interfacial interaction, and the viscoelastic properties of the blend components (Vanoene 1972; Wu 1987; Hemmati et al. 2001a, b; Tchomakov et al. 2004; Paul 2012). The morphology of the binary polymer blends can consist of droplets of one phase in the other phase or of two continuous phases forming co-continuous microstructure. In ternary blends consisting of three immiscible polymeric components, various types of morphology can develop; separately dispersion of the minor phases in the major phase and encapsulation of one minor component by the other one in the matrix phase, known as core-shell morphology (Horiuchi et al. 1997, Horiuchi and Nakayama 1999; Wilkinson et al. 1999; Reignier et al. 2003; Valera et al. 2006; Zhang et al. 2007; Ravati and Favis 2010). The interfacial tension between different phases, viscosity, and elasticity ratios of the components and the extent of deformation flow field are the most effective factors on the type of morphology (Favis 1990; Valera et al. 2006; Zhou et al. 2013). In other words, the morphology of binary as well as ternary blends is influenced by kinetic and thermodynamic factors. It has also been well known that rheological and mechanical properties of polymer blends are greatly influenced by the developed morphology during the mixing process (Salehiyan and Ray 2018).

The morphology of the ternary blends can be predicted through the knowledge of interfacial tension between different components. The balance of interfacial forces has been represented in terms of spreading coefficient by Hobbs et al. (1988) for a ternary blend in which two distinct polymers ($i$ and $j$) are dispersed in a major matrix phase ($k$)

✉ Bahareh Afsari
   bahareh.afsari68@gmail.com

✉ Mir Karim Razavi Aghjeh
   karimrazavi@sut.ac.ir

1   Institute of Polymeric Materials, Sahand University of Technology, Sahand New Town, Tabriz P.C.: 51335-1996, Iran

2   Faculty of Polymer Engineering, Sahand University of Technology, Sahand New Town, Tabriz P.C.: 51335-1996, Iran

$$\lambda_{ij} = \alpha_{jk} - \alpha_{ik} - \alpha_{ij} \tag{1}$$

where $\alpha_{ij}$ is the interfacial tension between **i** and **j** components and $\lambda_{ij}$ is referred to as the spreading coefficient of polymer **i** to encapsulate polymer **j**. According to the signs of the spreading coefficients, for a given matrix, four types of morphologies can be observed. $\lambda_{ij}$ must be positive to provide an interfacial driving force by component **i** to encapsulate component **j**. If both $\lambda_{ij}$ and $\lambda_{ji}$ are negative, components of **j** and **i** will tend to form isolated dispersed phases in matrix **k**. Another phenomenological model to predict the morphology of the ternary blends has been developed by Guo et al. (1997a) called minimum free energy model. The authors concluded that the free energy of mixing of a multiphase blend is a function of the interfacial area and interfacial tension between each pair of the components. Comparing the interfacial energies of the different possible structures, the most stable morphology corresponds to the minimal free energy of mixing of various morphologies. For any type of morphology, the free energy of mixing can be written as

$$G = \sum_i n_i \mu_i + \sum_{i \neq j} A_{ij} \alpha_{ij} \tag{2}$$

where $G$ is Gibbs free energy; $n$, the number of moles; $\mu$, the chemical potential; $\alpha$, the interfacial tension; and $A_i$, the interfacial area. The first term of Eq. 2 is equal for all types of morphologies, and therefore, the difference between different morphologies would be the difference between the second terms. Guo et al. (1997a) extended the second term of the equation as relative interfacial energy (RIE) for different cases as

$$\left(\sum A_i \alpha_{ij}\right)_{B+C} = (4\pi)^{1/3} \left[ n_B^{1/3} x^{2/3} \alpha_{AB} + n_C^{1/3} \alpha_{AC} \right]$$
$$\times (3V_C)^{2/3} \tag{3}$$

$$\left(\sum A_i \alpha_{ij}\right)_{B/C}$$
$$= (4\pi)^{1/3} \left[ n_B^{1/3}(1+x)^{2/3} \alpha_{AB} n_C^{1/3} \alpha_{BC} \right] (3V_C)^{2/3} \tag{4}$$

$$\left(\sum A_i \alpha_{ij}\right)_{C/B}$$
$$= (4\pi)^{1/3} \left[ n_B^{1/3} x^{2/3} \alpha_{BC} + n_C^{1/3}(1+x)^{2/3} \alpha_{AC} \right]$$
$$\times (3V_C)^{2/3} \tag{5}$$

By assumption $n_B = n_C$, the modified relative interfacial energy (RIE) equations can be written as follows:

$$(\text{RIE})_{B+C} = \left(\sum A_i \alpha_{ij}\right)_{B+C}/k = x^{2/3} \alpha_{AB} + \alpha_{AC} \tag{6}$$

$$(\text{RIE})_{B/C} = \left(\sum A_i \alpha_{ij}\right)_{B/C}/k = (1+x)^{2/3} \alpha_{AB} + \alpha_{BC} \tag{7}$$

$$(\text{RIE})_{C/B} = \left(\sum A_i \alpha_{ij}\right)_{C/B}/k = x^{2/3} \alpha_{BC} + (1+x)^{2/3} \alpha_{AC} \tag{8}$$

$k$ is a constant calculated as $k = 3\sqrt{4\pi} \times 3\sqrt{n_C} \times (3V_C)^{2/3}$; $x$ is defined as $x = V_B/V_C$; $V_i$ is the volume of each phase; and $n_B$ and $n_C$ are the numbers of particle phases of $B$ and $C$ phases, respectively.

The resultant morphology in ternary blends exerts basic changes on the rheological properties (Codou et al. 2018). The rheological properties of immiscible blends have been extensively studied from both experimental and theoretical points of view (Palierne 1990; Guo et al. 1997b). Rheological studies on the interfacial properties of polymer blends are based on the fact that heterogonous polymer blends in the molten state behave as an emulsion (Riemann et al. 1996, 1997; Shi et al. 2002). The deformability of the dispersed droplets is a characteristic of emulsions. The equilibrium shape of the dispersed inclusions in a matrix phase is determined by two types of force: the viscous forces outside the particles and the Laplace pressure originating from interfacial tension. Reformation of the deformed droplets to their primary spherical shape is a process called the "form relaxation" (Graebling et al. 1993a; Riemann et al. 1996, 1997; Jacobs et al. 1999). This relaxation process manifests itself as a relaxation peak in the relaxation time spectra at times longer than the relaxation time of each of the blend components (Riemann et al. 1996, 1997, Horiuchi et al. 1997; Shi et al. 2006). Moreover, the addition of block or graft copolymers as compatibilizers, even at low volume fractions, leads to the detection of another relaxation process with a longer relaxation time than the form relaxation time (Palierne 1990; Graebling et al. 1993b; Riemann et al. 1996, 1997; Silva et al. 2010). Riemann et al. (1997) studied this long relaxation time mechanism for PS/PMMA 7.5/92.5 blend compatibilized by 1.0 wt% of symmetric diblock copolymer, P(S-b-MMA) and P(CHMA-b-MMA). Jacobs et al. (1999) observed a slow relaxation process in small amplitude oscillatory shear experiments with a compatibilizer of different molecular structure on the PS/PMMA blends. Unlike Riemann et al. (1997) and Jacobs et al. (1999), Velankar et al. (2001) did not report this slow interfacial relaxation process in the PDMS/PIB blends. Shi et al. (2002, 2006) investigated the terminal relaxation time theoretically and experimentally in PP/PP-g-MA/PA6 ternary blends based on an emulsion-in-emulsion morphology model.

In the PP/PA6/EPDM-g-MA ternary system, the EPDM-g-MA rubbery phase plays the roles of compatibilizer and toughener, simultaneously, as the EPDM-g-PA copolymer is in situ formed during the melt mixing process (Lee et al. 2009; Li et al. 2012; Shokoohi et al. 2012; Zhou et al. 2013; Yin et al. 2013; Dou et al. 2015; Salehiyan and Ray 2018). The compatibilizing effect of EPDM-g-MA would be taking place even at very low contents up to some extents above which the independent toughener role of EPDM-g-PA is detected. The main objective of the present work was to investigate the morphology of reactive PP/PA6/EPDM-g-MA ternary blends at relatively low EPDM-g-MA contents to determine the weight fraction of the rubbery phase in which the

dispersed PA6 particles are completely encapsulated. Besides, the shell formation process in reactive PP/PA6/EPDM-g-MA ternary blends was studied via quantification of the morphology alteration as a function of EPDM-g-MA content. The morphology changes were followed by linear viscoelastic properties of the ternary systems and their corresponding reference samples. In this ternary reactive system, the form and the interfacial relaxation processes were also evaluated, and the results were correlated to the morphology. The stability of the morphology of these ternary systems during rheological analysis was also studied. The effect of gradual shell development on the fracture behavior of this ternary system has previously been studied (Hasanpour et al. 2019).

# Experimental

## Materials

Polyamide 6 (PA6, with a density of 1.13 g/cm$^3$ and melting temperature of 223 °C) used in this study was Tecomid NB40 NL E. The isotactic polypropylene (iPP) (MFI = 5.0 g/10 min at 2.16 kg and 230 °C and melting temperature of 165 °C) was obtained from Polynar Petrochemical Co., Tabriz, Iran. Ethylene-propylene-diene rubber grafted with maleic anhydride (EPDM-g-MA, denoted as mEPDM hereinafter), with the trademark of TRD-359EP, was purchased from Yangzhou Henghui Chemical Co., Ltd, with Moony viscosity (ML 1 + 4, 100 °C) of 23, mass density of 0.875 g/cm$^3$, and MAH content of about 1.2 wt%.

## Blending and sample preparation

To avoid the effect of moisture, all the materials were dried in a vacuum oven at 80 °C for 12 h prior to mixing. All the ternary blends were prepared in an internal mixer (Brabender W50EHT) with a rotor speed of 60 rpm at starting temperature of 230 °C for 8 min. The PP and PA6 phases were melt-blended for about 3 min, and then, the EPDM-g-MA phase was added into the melt mixture and compounding was continued for 5 min more. The same processing conditions were applied for the pure polymeric materials and binary blends as reference samples. The weight ratio of PP/PA6 was kept constant at 80/20 in PP/PA6 binary blend and PP/PA6/EPDM-g-MA ternary blends. In ternary blends, the weight ratio of the EPDM-g-MA phase was varied from 0.5 to 9.0 wt% based on the whole blend. This type of composition arrangement was chosen to keep the PP/PA6 ratio constant in order to eliminate the effect of the PP/PA6 ratio on the morphology. A small amount of the prepared blend samples was rapidly quenched in liquid nitrogen for morphological studies, and what remained was compression molded into suitable pieces for rheometry analysis. Molding was carried out at 230 °C followed by slow water cooling under low pressure.

## Morphological observations

Morphology of all the blends was characterized by field emission scanning electron microscopy (FESEM; Mira 3-XMU). The blend samples were cryogenically fractured in liquid nitrogen, and selective extraction using cyclohexane at 50 °C for 24 h was applied to the EPDM-g-MA phase domains. The samples were then dried at 85 °C in a vacuum oven overnight and gold sputtered for good conductivity of the electron beam, and microphotographs were taken with different magnifications. The same procedure was also applied for the samples that underwent the time-sweep tests, discussed in "Rheological studies." The morphology of the dispersed phases was evaluated using the image analysis software (Image J 1.44p). The size distribution of the dispersed PA6 particles was determined by size measurements of approximately 300 particles.

## Rheological studies

The flow behavior and melt linear viscoelastic properties of different samples were investigated using a dynamic rheometer (MCR301, Anton Paar) equipped with a parallel plate configuration (diameter = 25 mm, gap = 1 mm). The dynamic frequency sweep tests were applied in the range of 0.04–625 rad/s at 230 °C and 1.0% strain amplitude to maintain the response of materials in the linear viscoelastic regime. In order to benefit the advantages of time-temperature superposition concept and to investigate the rheological properties in a wide range of frequencies, the frequency sweep tests were conducted in 230, 250, and 270 °C for some samples. The r-vGP plot (phase angle ($\delta$) versus the reduced absolute value of the complex modulus) was inquired by dynamic frequency sweep tests at 230, 250, and 270 °C temperatures for the blend with 7.0 wt% rubbery phase. To study the morphology stability, dynamic time sweep tests were applied for some compositions at constant frequency of 0.05 Hz and 1.0% strain amplitude. To clarify the effect of morphology instability and possible phase degradation on rheological properties, the same experiments were also applied for neat PP, PP/PA6 blends and the blends containing 3.5 to 9.0 wt% EPDM-g-MA at 270 °C.

## FTIR analysis

Infrared absorption spectroscopy (ISS88, Bruker Germany) was used to evaluate the reaction between NH groups of PA6 and MA groups of EPDEM-g-MA. All the samples were compression molded into a thin layer of films at 230 °C and about 3.0 MPa pressure. The samples were cooled to room temperature in the mold under pressure, and then scanning in the range of 400–4000 cm$^{-1}$ was applied.

**Table 1** Contact angle and surface energy values of the components

| Sample | Contact angle (°) | | Surface tension (mN/m) at 25 °C | | | Surface tension (mN/m) at 230 °C |
|---|---|---|---|---|---|---|
| | Water | Diiodomethane | Total $(\gamma)$ | Dispersion component $(\gamma^d)$ | Polar component $(\gamma^p)$ | Total $(\gamma)$ |
| PP | 106.5 | 66 | 29.1 | 28.51 | 0.59 | 17.62 |
| PA6 | 61.3 | 29.1 | 51.7 | 32.94 | 18.76 | 38.37 |
| mEPDM | 88.8 | 42.2 | 39.2 | 33.26 | 5.94 | 27.70 |

# Results and discussion

## Interfacial tension, morphology prediction

The interfacial tension and spreading coefficient values at processing temperature, calculated from the surface tension data and presented in our previous works (Mazidi et al. 2015, 2016), are listed in Table 1.

The data in Table 1 demonstrate that the interfacial tension value for PP/PA6 is much larger than those of the other polymer pairs. In the case of reactive PP/PA6/EPDM-g-MA ternary blends, interfacial tension values for PP/PA6 and PA6/EPDM-g-MA are also higher than that of PP/EPDM-g-MA. Using the data reported in Table 1 and Eqs. 6 to 8, the RIE values were calculated and the results are presented in Tables 2 and 3. As the results of Tables 2 and 3 show, the spreading coefficient values for reactively compatibilized ternary blends suggest complete encapsulation morphology with EPDM-g-MA and PA6 forming the shell and core phases, respectively. It should be noted that the interfacial tensions of polymer pairs can significantly be changed by in situ reaction at the interfacial region during the reactive blending (Shi et al. 2002; Wilkinson et al. 2004; Krache et al. 2004; Omonov et al. 2005; Purnima et al. 2006; Wang et al. 2011, Wang and Xie 2006; Díaz et al. 2007; Lee et al. 2009; Jazani et al. 2011, 2013; Shokoohi et al. 2012; Li et al. 2012; Zhou et al. 2013; Rastin et al. 2014; Salehiyan and Ray 2018). This means that by considering the chemical reaction of EPDM-g-MA with PA6 macromolecular chains, the actual interfacial tension value for the PA6/EPDM-g-MA pair in the reactive ternary systems would be much lower than that reported in Table 1. It can also be seen that the results are in agreement with the results of spreading coefficient measurements by means that the minimum value of the free energy appertains to the morphology in which the rubbery phase has encapsulated the PA6 particles.

## Blend morphology

Figure 1 shows the FESEM images of cryogenically fractured cross-section surfaces of different blends containing various amounts of EPDM-g-MA. For uncompatibilized PP/PA6

blend (Fig. 1a), the typical matrix/dispersed morphology characteristic of immiscible binary blends is observed. The coarse particle size distribution of dispersed domains of PA6 phase and the smooth interface without any visible roughness between the phases are indicative of high interfacial tension between the components. The poor interfacial bonding in this system leads to PA6 particles being separated from the matrix phase, leaving holes on the fracture surface under the fast-cryogenic fracture or lying loose on the surface (Mazidi et al. 2016). Upon addition of EPDM-g-MA as a reactive compatibilizer precursor with subsequent formation of PA-g-EPDM graft copolymer at the blend interface, the morphology starts to change. Further application of the compatibilizer improves the interfacial adhesion between the phases and makes the droplets smaller. In all the compatibilized blends (Fig. 1b–e), the size reduction of the PA6 droplets is clearly seen. Moreover, a lot of small dark holes in higher magnification inside Fig. 1c can be seen which are attributed to the small composite droplets extracted in the etching process. These observations are in good consistency with the theoretical predictions of phase morphology based on spreading coefficient and minimum free energy concepts, presented in the previous section. Figure 2 depicts FESEM micrographs of some PP/PA6/EPDM-g-MA ternary blends at two different higher magnifications. According to these micrographs, compatibilization with 5.0 wt% or higher EPDM-g-MA causes the adjacent particles to come closer to each other along with a further decrease in droplet size. The samples show a morphological feature in which the minor phases form well-defined clusters, shown by arrows, dispersed in the PP matrix. It is expected that the development of such microstructures would influentially affect the viscoelastic properties of the system.

## Quantification of the PA6 droplet size

The number-average radius, $R_n$, and volume-average radius, $R_v$, as well as the distribution of the particle size, $\overline{R_v}/\overline{R_n}$, were calculated for the dispersed PA6 core, and the results are presented in Table 4. The number-average radius, $R_n$, was also plotted versus EPDM-g-MA content in Fig. 3.

**Table 2** Interfacial tension of each pair of the components and the calculated spreading coefficient value

| Polymer pairs | Interfacial tension, $\gamma_{ij}$ (mN/m), at 230 °C | Spreading coefficient, $\lambda_{ij}$ |
|---|---|---|
| PP/PA6 | 14.1 | $\lambda_{AB} < 0$ |
| PP/mEPDM | 4.2 | |
| PA6/mEPDM | 5.3 | $\lambda_{BC} < 0$, $\lambda_{CB} > 0$ |

*A* PP, *B* PA6, *C* mEPDM

The plot in Fig. 3 has the typical shape of an emulsification curve up to 7.0 wt% of the EPDM-g-MA phase above which the PA6 particle size increases. The sharp reduction in the minor phase size upon addition of a small amount of interfacial agent is explained in terms of reduction in interfacial tension and the extent of coalescence of the droplets. However, further increase in EPDM-g-MA content to 9.0 wt% led to a slight increase in PA6 droplet size. This is in contrast to the interfacial tension data and seems to be unexpected at first glance. This observation can be justified as follows: the morphology of this ternary system is influenced by two different competitive roles of the EPDM-g-MA rubbery phase. An increase in EPDM-g-MA content would simultaneously increase both the interfacial interaction between the PP and PA6 phases and the viscosity ratio of the composite droplet, as it exhibits a higher viscosity than the other two components. The former is beneficial for particle size reduction while the latter is in favor of increasing the composite droplet and PA6 particle sizes (Reignier and Favis 2003). Therefore, at EPDM-g-MA contents lower than shell completion concentration, the first effect is dominant, whereas at higher concentrations and after saturation of the interface, the second effect predominates and therefore the particle size increases upon addition of 9.0% of rubbery phase.

To evaluate the shell thickness of the EPDM-g-MA at composite droplets, an expression which is developed by Reignier and Favis (2000, 2003) and Valera et al. (2006) was used (Eq. 9):

$$H = \frac{1}{2} D_v \left[ 1 - \sqrt[3]{\left( 1 - \varphi_{\mathrm{mEPDM/DP}} \right)} \right] \tag{9}$$

$D_v$ refers to the volume average diameter of composite droplets, $\varphi_{\mathrm{mEPDM/DP}}$ refers to the volume fraction of EPDM-g-MA (based on the dispersed phases), and H is the shell thickness. The values of the EPDM-g-MA shell thickness for three blends before and after shell completion were calculated using the above expression and reported in Table 5.

The results indicate that a thin layer of rubbery phase has encapsulated the PA6 inclusions in the blend containing 2.5 wt% of EPDM-g-MA which has been doubled at 3.5 wt% of the compatibilizer. However, the shell thickness remains constant within considering the experimental error in 5.0 wt%. After the shell completion, the excess the EPDM-g-MA phase is dispersed as a third phase owing to its low interfacial tension with the matrix phase. The presence of such inclusions induces the coalescence between the separated droplets of covered PA6 particles, which results in the cluster formation of composite droplets in high contents of the compatibilizer. These consequences have also been concluded in FESEM micrographs. In weight fractions higher than 5.0 wt% of EPDM-g-MA, the existence of clusters causes errors in the calculation of theoretical thickness via Eq. 9.

## Rheological characterizations

Rheological behaviors of PP, PA6, and PP/PA6 blend are presented in Fig. 4. It is apparent that neat polymers display a Newtonian plateau behavior at low-frequency regions. As expected, for PP/PA6 blend, an increase in the elastic modulus particularly at low frequency ranges is observed which is attributed to the shape relaxation of the dispersed droplets of PA6 minor phase.

The storage modulus and damping factor for PP/PA6/EPDM-g-MA ternary blends containing different amounts of EPDM-g-MA are compared in Fig. 5. It can be seen that the storage modulus of the ternary blends are less affected at low EPDM-g-MA contents even at low frequency ranges, but it starts to monotonically increase up to some EPDM-g-MA contents (~ 5.0 wt%) above which an appreciable increase in the storage modulus at low frequencies has taken place. During the melt mixing process, the maleic anhydride groups of EPDM-g-MA would chemically react with the amine end groups and/or amide linkages of the PA6 chains leading to the generation of the PA-g-EPDM compatibilizer copolymer at the interfacial region, which could strongly enhance the interfacial interaction between the PP and PA6 phases (Fig. 5a). The same results can be elucidated from damping factor data where the results clearly show that the damping factor monotonically decreases at low

**Table 3** Morphology predicted by minimal surface energy

| Supposed morphology | Relative interfacial energy (RIE) (mN/m) |
|---|---|
| B + C | 15.3 |
| B/C | 17 |
| C/B | 9.9 |

*A* PP, *B* PA6, *C* mEPDM

**Fig. 1** FESEM micrographs of PP/PA6/EPDM-g-MA (80/20/$x$) w/w ternary blends compatibilized with **a** 0%, **b** 2.5%, **c** 3.5%, **d** 5%, **e** 7%, and **f** 9% EPDM-g-MA. EPDM-g-MA phase has been etched
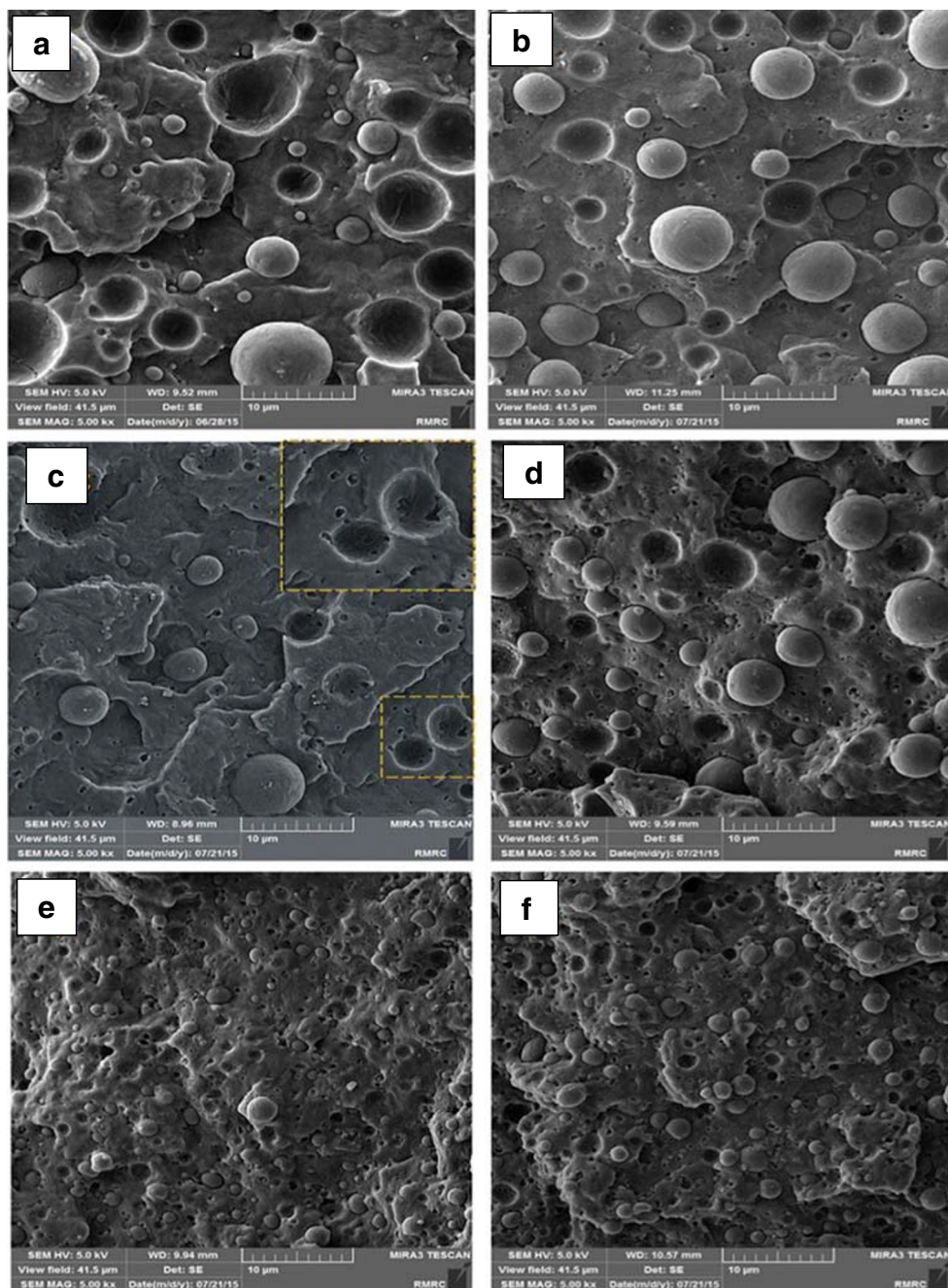


frequencies with EPDM-g-MA content above which the variation trend of the damping factor displays characteristic of pseudo solid-like behavior at high EPDM-g-MA contents (Fig. 5b). This alteration in rheological properties (a plateau in the storage modulus and a maximum in the damping factor curve) at high EPDM-g-MA contents can be related to the alteration in morphological characteristics of the resulted ternary blends. The decreased damping capability of uncompatibilized PP/PA6 blend compared to the neat polymers, especially at low frequencies, is related to shape relaxation of PA6 droplets. In the case of compatibilized blends, flat damping peaks can be observed at low frequencies and the relaxation potential of the material is further decreased compared to the uncompatibilized blend. This originates from the greater interactions at the interface region according to the further application of the compatibilizer in blends. The lowest values of the damping factor in the frequency ranges corresponding to the terminal region are seen in the blends inclusive 7.0 and 9.0 wt% compatibilizer. These blends highlight the biggest increase in elasticity through the decreasing of the size of the dispersed phase that arises from the decreasing of the interfacial tension.

**Fig. 2** FESEM micrographs of shell thickness changing and promotion of aggregations as a function of **a**, **b** 5%; **c**, **d** 7%; and **e**, **f** 9% EPDM-g-MA. EPDM-g-MA phase has been etched
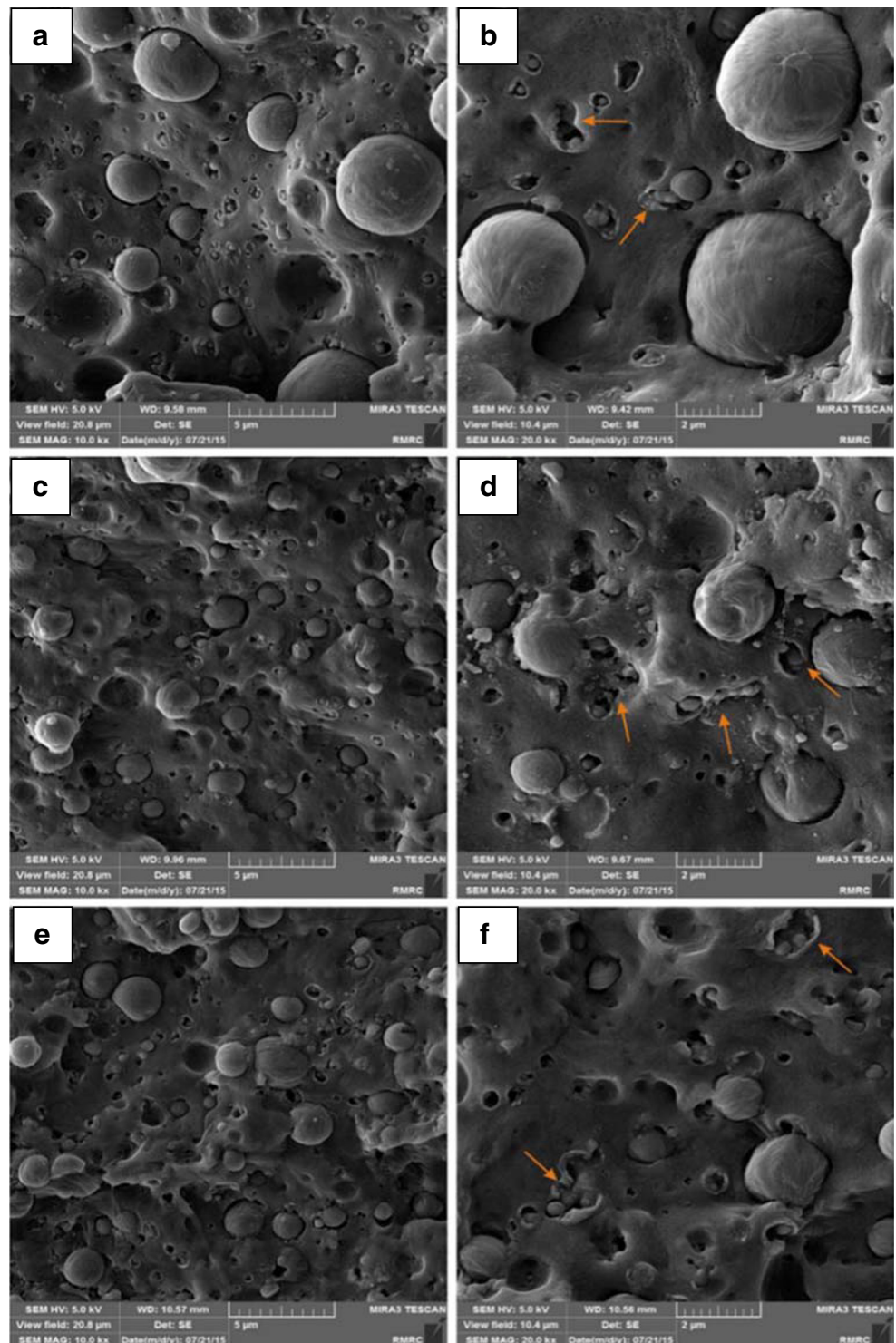


To further clarify the EPDM-g-MA content in which the possible morphology alteration had taken place, the ratio of the storage modulus value at the lowest and the highest angular frequency is plotted versus EPDM-g-MA weight fraction in Fig. 6. The results clearly show that at about 5.0 wt% of EPDM-g-MA, the linear dependency of this ratio changes to exponentially one which is a collaboration of morphology alteration at this concentration.

Morphological features of multiphase systems can better be reflected in the results of Cole-Cole plots (Sundararaj and Macosko 1995; Li et al. 2006; Codou et al. 2018). Using these results, various relaxation processes including relaxation of

**Table 4** Number-average, volume-average, and distribution of the PA6 droplet radius

| Sample | $\overline{R_n}$ | $R_v$ | $\overline{R_v}/\overline{R_n}$ |
|---|---|---|---|
| PP/PA6/mEPDM—80/20/0 | 1.69 | 3.077 | 1.82 |
| PP/PA6/mEPDM—80/20/1.5 | 1.38 | 2.391 | 1.73 |
| PP/PA6/mEPDM—80/20/2.5 | 1.32 | 2.283 | 1.73 |
| PP/PA6/mEPDM—80/20/3.5 | 1.15 | 1.890 | 1.64 |
| PP/PA6/mEPDM—80/20/5 | 1.09 | 1.750 | 1.61 |
| PP/PA6/mEPDM—80/20/7 | 0.62 | 0.880 | 1.42 |
| PP/PA6/mEPDM—80/20/9 | 0.70 | 1.057 | 1.51 |

polymer chains, shape relaxation of dispersed droplets, and interfacial relaxations can be deconvoluted (Marin et al. 1975; Ajji et al. 1988; Li et al. 2006; Basseri et al. 2014; Codou et al. 2018). Figure 7 illustrates the Cole-Cole plots for all the blends and neat PP. At high frequencies (at low values of $\eta'$), the neat PP exhibits a typical semicircle curve, characteristic of unimodal molecular weight distribution of this polymer. For the binary blends, an additional peak at the low-frequency region (at high values of $\eta'$) depicts the relaxation of the droplets. Shifting of this peak to the lower frequencies together with its broadening is the result of shape relaxation of the smaller droplets in blends containing various amounts of compatibilizer. Moreover, the relaxation curves associated with polymer chains and shape recovery have overlapped, leading to the appearance of a single wide curve. Additionally, for the blends containing higher than 5.0 wt% of EPDM-g-MA, the presence of a tail beside the main peak at very low frequencies is attributed to another relaxation
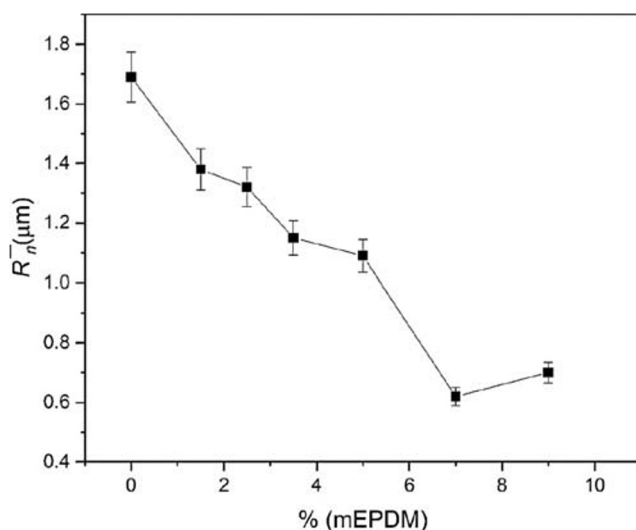


**Fig. 3** Number average radius $\overline{R_n}$ of PA6 droplets in PP/PA6/EPDM-g-MA (80/20/0-9) w/w ternary blends with different weight fractions of EPDM-g-MA

mechanism in the compatibilized blends. The origin of this additional relaxation phenomenon would be more evident in the weighted relaxation spectra.

Another effective method to evaluate relaxation times interdependent to microstructure in polymer blends is the weighted relaxation time spectra (Gramespacher and Meissner 1992; Sundararaj and Macosko 1995; Vinckier et al. 1996; Liu et al. 2006). The continuous relaxation spectrum, $H(\tau)$, was determined by fitting experimental $G'(\omega)$ and $G''(\omega)$ data in accordance with the numerical differentiation procedure developed by Ninomiya and Ferry (1959). The sensitivity of the $H(\tau)$ plot to the relaxation of the blend interface is not strong enough. Therefore, the weighted relaxation spectrum, $\tau H(\tau)$, versus $\tau$ is usually used to clearly separate the relaxation times of the interface from the contribution of the components (López-Barrón and Macosko 2012). The weighted relaxation spectra for all the blends and the PP component are demonstrated in Fig. 8. A peak in the spectra is observed for all the blends at a relaxation time of about 0.05 s. This peak is obviously associated with the relaxation of PP matrix chains. Extra relaxation peaks are seen at longer times. A second peak in the relaxation spectrum is observed for all the compatibilized and uncompatibilized blends due to the relaxation of the droplets. In this plot, based on Vinckier's assumption (1996), the magnitude of the peak is related to the amount of interfacial area, while the time of the peak is dependent on the size of the droplets (López-Barrón and Macosko 2012).

Application of the different amounts of compatibilizer altered droplet size as shown in Figs. 1 and 2. It is seen in Fig. 8 that the highest $\tau H(\tau)$ value relates to 7.0 wt% compatibilized blend which is consistent with the minimum droplet size obtained in this composition corresponding to the larger interfacial area. Moreover, a decreased intensity of the $\tau H(\tau)$ value for 9.0 wt% compatibilized blend compared to 7.0 wt% compatibilized blend is an indication of increased dispersed particle size. The results also show that the form relaxation times of compatibilized blends are shifted towards shorter

**Table 5** Theoretical calculation of shell thickens

| Sample | mEPDM weight fraction % mEPDM | Volume fraction of mEPDM (based on the dispersed phase) % $\varphi_{mEPDM/DP}$ | Shell thickness, $H$ (μm) |
|---|---|---|---|
| PP/PA6/mEPDM—80/20/2.5 | 2.5 | 14.2 | 0.114 |
| PP/PA6/mEPDM—80/20/3.5 | 3.5 | 18.9 | 0.244 |
| PP/PA6/mEPDM—80/20/5 | 5.0 | 36.3 | 0.245 |

times with increasing the EPDM-g-MA content up to 3.5 wt% due to less deformation related to smaller inclusions which lead to faster reformation process. Droplet sizes in different compositions, obtained via morphological analysis (Fig. 1), together with their corresponding shape relaxation times, elicited from weighted relaxation time spectra, are presented in Table 6. For the blends containing higher than 3.5 wt% of EPDM-g-MA, the shift of relaxation times to longer times is a consequence of fully surrounded PA6 droplets by a thick rubbery phase which postpones the recovery of the deformed droplets. Analysis of the relaxation time spectra of the compatibilized blends demonstrates that there is an additional relaxation peak other than the form relaxation peak associated with terminal relaxation processes. For all the compatibilized blends, only a tail in the right-hand side of the relaxation spectra was observed (Fig. 8). This additional relaxation time is assigned to a non-isotropic interfacial stress, which may arise from relaxation processes of the graft copolymers at the interface. The appearance of this characteristic relaxation time was first described by Riemann et al. (1996).

The presence of a proper compatibilizer as an interface modifier surely affects the deformation and the droplet break-up behaviors by reducing the interfacial tension and therefore
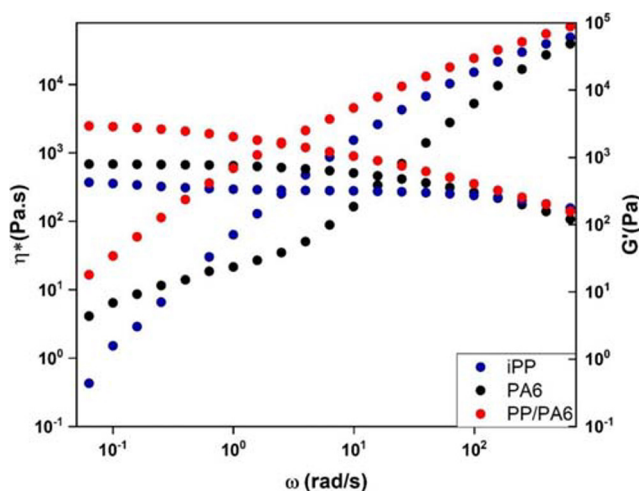
lowers the values of hydrodynamic stress at which the drops of a certain size are broken (Stone and Leal 1990; Pawar and Stebe 1996; Li and Pozrikidis 1997; Salehiyan and Ray 2018). Numerical simulations have shown a much more complicated picture in which the bulk flow induces gradients in the
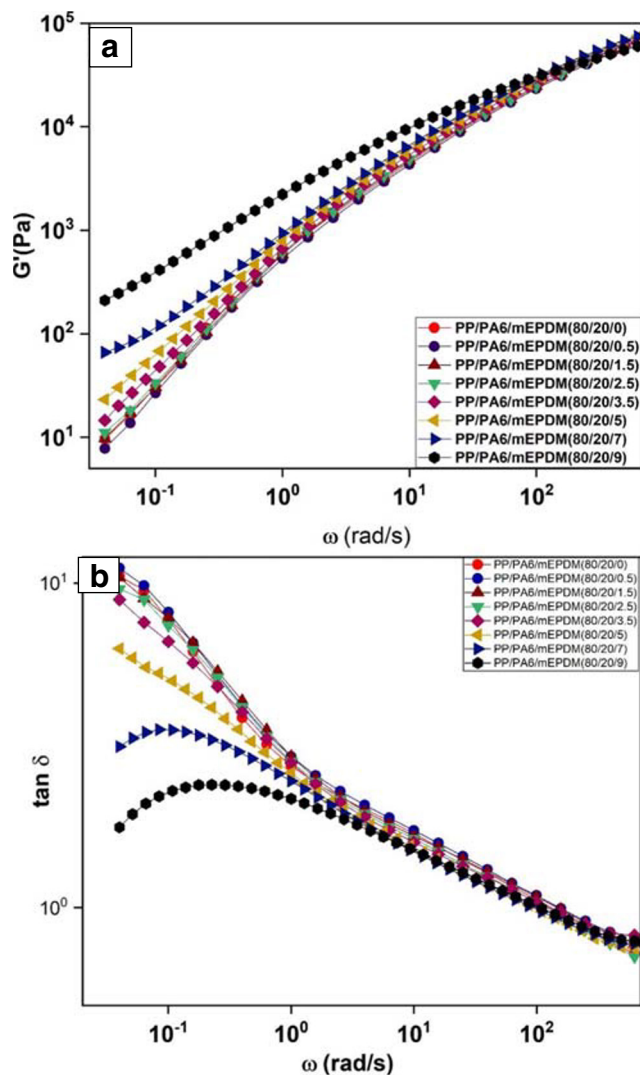


**Fig. 5** Alteration of **a** storage modulus of PP/PA6/EPDM-g-MA ternary blends with various amounts of compatibilizer (80/20/0-9) w/w; **b** damping factor of PP/PA6/EPDM-g-MA (80/20/0-9) w/w ternary blends vs. angular frequency at 230 °C
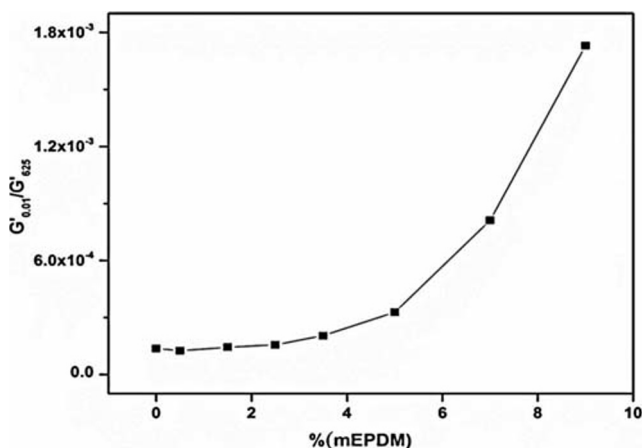


**Fig. 4** Evaluation of storage modulus ($G'$) and complex viscosity ($\eta^*$) with angular frequency at 230 °C in pure PP, PA6, and their binary blend PP/PA6 (80/20) w/w

Fig. 6 Normalized storage modulus vs. weight fraction of EPDM-g-MA



Fig. 8 Weighted relaxation spectrum of PP neat component and compatibilized ternary blends containing different amounts of EPDM-g-MA at 230 °C

concentration ($C_s$) of the compatibilizer along the drops' surface. When the parameter ($\frac{\partial \alpha}{\partial C_s}$) is large, this gradient in the interfacial tension can greatly generate along the surface. As a consequence, the deformation followed by local deformation of the interface causes a decrease in the local compatibilizer concentration and breakup characteristics of the droplet (Van Puyvelde et al. 2001). In some cases, compatibilized drops even displayed widening, i.e., the dimension along the vorticity direction was larger than the original droplet diameter. Interfacial tension gradient and/or suppression of interfacial slippage was considered to be the likely cause of this widening. In fact, as it is shown in Fig. 9a when droplets undergo the extensional flow, bulk flow drives the compatibilizer towards the ends of the droplet causing a gradient in the interfacial tension along the droplet surface. The lower interfacial tension at the tips progresses tip streaming as demonstrated in Fig. 9c which tends to reduce the critical capillary number ($Ca_{cr}$). This tendency would be opposed by Marangoni stresses (white arrows). In shear flow, these effects are combined with
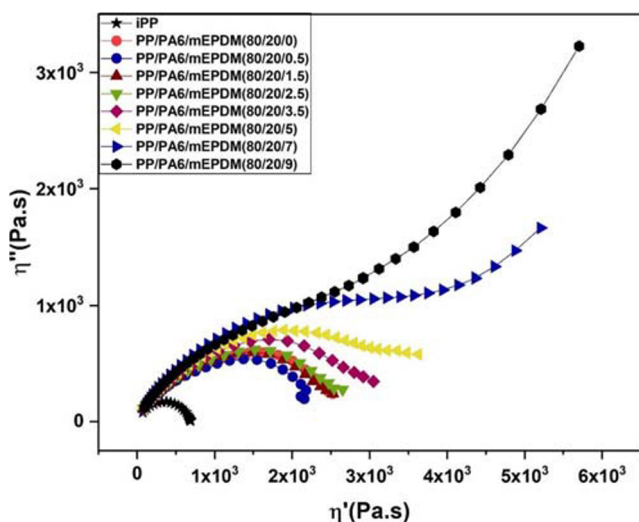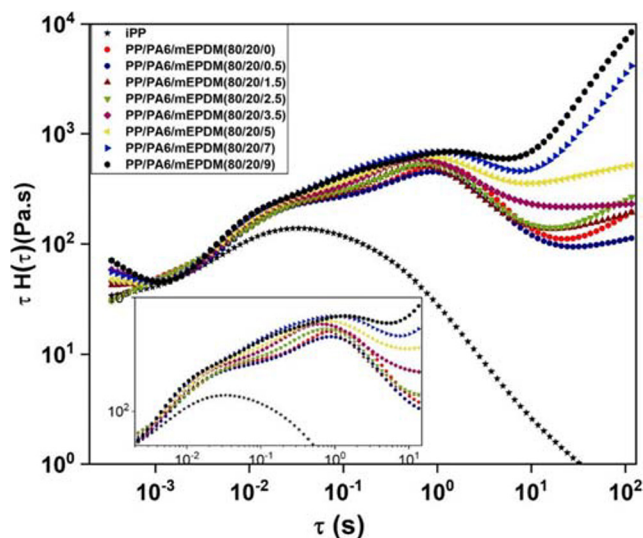
rotation of droplets (Fig. 9b). However, diffusion of long chains of compatibilizer is supposed to have a negligible effect in these systems (Pawar and Stebe 1996). The change in the situation of the tails with the amount of graft copolymer at the interface can be noticed from Fig. 8. However, this relaxation time is less influenced by the interfacial tension (Riemann et al. 1997). This phenomenon is mainly governed by an additional contribution, the interfacial shear modulus, characterized by the height of the tails. Increasing in the range of the considered concentrations is a consequence of the rigidification of the interface of the droplets. The interface shear modulus plays the role and acts against the deformation of the interface, if a deformation is applied to the blend and consequently to the interface. The evidence of interfacial viscoelastic effects in immiscible polymer blends has been limited to observation of a slow relaxation process $\tau_2$ (long time scales) in small amplitude oscillatory shear experiments of the blends with added compatibilizer (Riemann et al. 1996, 1997).



Fig. 7 Cole-Cole curve for PP and the PP/PA6/EPDM-g-MA (80/20/0-9) w/w ternary blends at 230 °C

**Table 6** Shape relaxation times alteration of droplets as a function of EPDM-g-MA content

| Blend | mEPDM (wt%) | $R_v$ (μm) | $\tau_1$ (s)[a] |
| --- | --- | --- | --- |
| PP/PA6/mEPDM (80/20/0) | 0.0 | 3.07 | 1.24 |
| PP/PA6/mEPDM (80/20/0.5) | 0.5 | 3.00 | 0.98 |
| PP/PA6/mEPDM (80/20/1.5) | 1.5 | 2.39 | 0.67 |
| PP/PA6/mEPDM (80/20/2.5) | 2.5 | 2.28 | 0.67 |
| PP/PA6/mEPDM (80/20/3.5) | 3.5 | 1.89 | 0.58 |
| PP/PA6/mEPDM (80/20/5) | 5.0 | 1.75 | 0.78 |
| PP/PA6/mEPDM (80/20/7) | 7.0 | 0.88 | 1.38 |
| PP/PA6/mEPDM (80/20/9) | 9.0 | 1.06 | 1.59 |

[a] $\tau_1$ is the characteristic time of dispersed phase form relaxation

**Fig. 9** Effects of graft copolymers on drop deformation, **a** extensional flow, **b** shear flow, **c** drop breakup due to the gathering of the compatibilizer at the drop tips
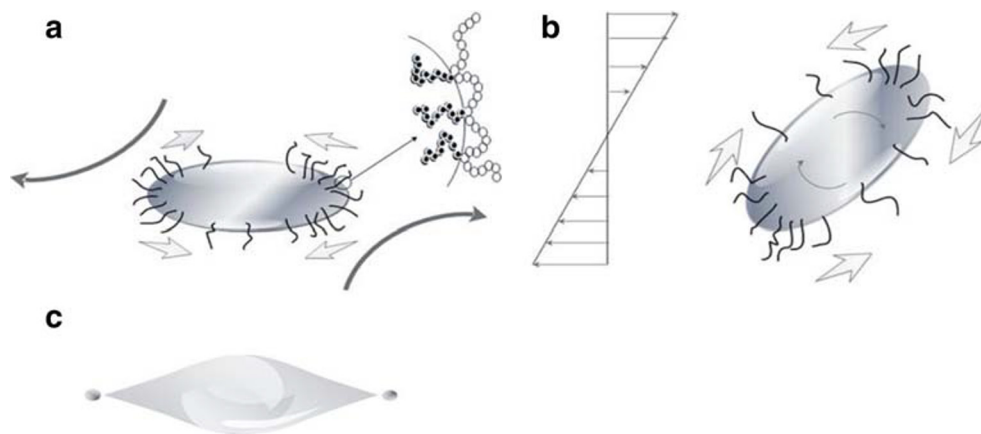
For the blends with compatibilizer contents less than 5.0 wt%, the tails in the right hand side of the relaxation spectra lead to zero trough the time while in the further weight fractions of compatibilizer (7.0 and 9.0 wt%) the long immortal tails suggested that the relaxations associated with the tails may be attributed to a network relaxation of the continuous structure (Li et al. 2006). It is believed that this behavior is due to the formation of droplet aggregation in these compositions.

### Morphological stability, effective parameters

The frequency sweep test for the ternary blend sample containing 7 wt% rubbery phase was applied in three different temperatures (230, 250, and 270 °C). Figure 10 shows the storage modulus of the sample at three different temperatures. The results clearly show that the rheological behavior of the sample at low angular frequency ranges changes, representative of probable alteration in the microstructure of the material at elevated temperatures. To get more insight into the subject, the r-vGP plot for the sample was considered. Regardless of the chemical constitution of the components or chemical topology, a reduced
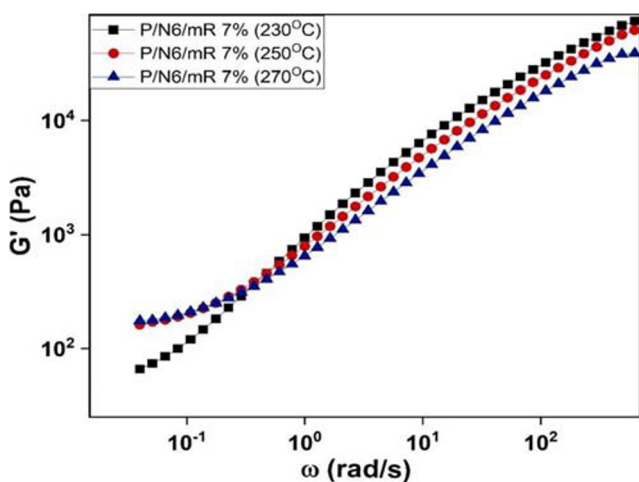
van Gurp−Palmen (r-vGP) plot was adopted to plot the phase angle ($\delta$) versus the reduced absolute value of the complex modulus, $|G*(\omega)|/G^o_N$, where $G^o_N$ is the plateau modulus. Here, the plateau modulus, $G^o_N$, was determined by the crossover modulus-based method ($G^o_N = G_c' = G_c''$ at an angular frequency of $\omega = \omega_c$) (Liu et al. 2006; Seo and Seo 2018). Totally, in vGP plots, the $a_T$ shift factor and overlapping of the curves related to the different temperatures are not needed, and following the different curves to form a monolithic arc is the only criterion to show the thermal stability (Van Gurp and Palmen 1998; Martin et al. 2000; Dealy and Plazek 2009). Figure 11 highlights the results of dynamic rheological measurements on the studied blend sample. No matching among the curves is an indication of the fact that the morphology in this blend is not stable in different temperatures.

Thermal instability and/or morphological alteration at elevated temperatures and long times can be followed by oscillatory time sweep experiments (Mazzeo 2012). Figure 12 shows the normalized storage modulus (the ratio of storage modulus to the storage modulus at test starting time) of four blend samples along the time. For all the blends, proceeding evidences to structural changes with time can be seen. The
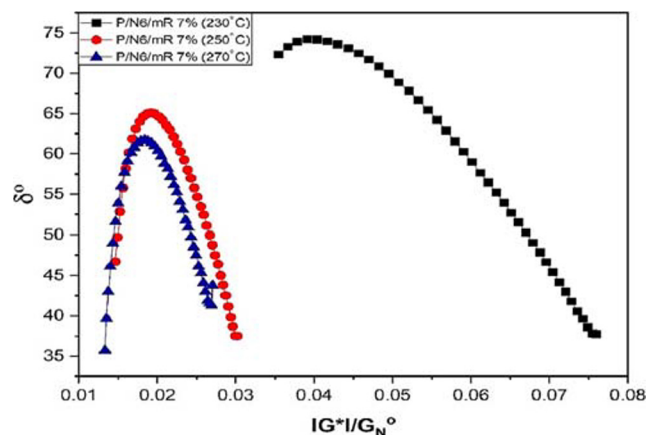


**Fig. 10** Alteration of storage modulus of PP/PA6/EPDM-g-MA (80/20/7) in three different temperatures



**Fig. 11** Variation of phase angle versus reduced absolute value of the complex modulus at different temperatures
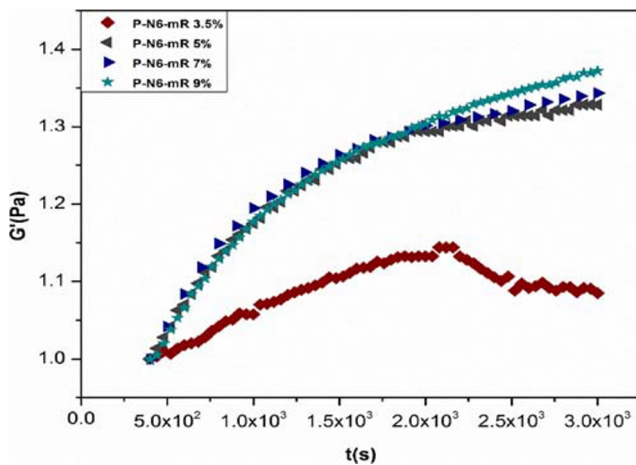
**Fig. 12** Time sweep test for blends containing over critical EPDM-g-MA content at 270 °C and 0.05 Hz

changes of storage modulus with the time for the blend containing 3.5 wt% compatibilizer are less than those of other blends containing higher compatibilizer contents. From these results, it can be concluded that the former blend exhibits more stability (chemical and/or morphological) than the latter blends. Some researchers have claimed that the hygroscopic nature of PA and its strong moisture absorption are the major difficulties of rheological characterization of the blends containing polyamides (Laun 1979; Khanna et al. 1996; Sailer 2008).

To evaluate the effect of the PA phase and PP matrix on the instability of the blends, time sweep experiments for PP/PA6 blend and neat PP at constant temperature of 270 °C were also conducted (Fig. 13), whereas in the case of PP/PA6 in which the $G'$ remained almost constant within measurement time, a monotonic decline was observed in the PP curve. The degradation of the PP chains as matrix phase even under the nitrogen atmosphere in the rheometer is the reason of decline of the storage modulus. Owing to the fact that the PP/PA6 ratio in all
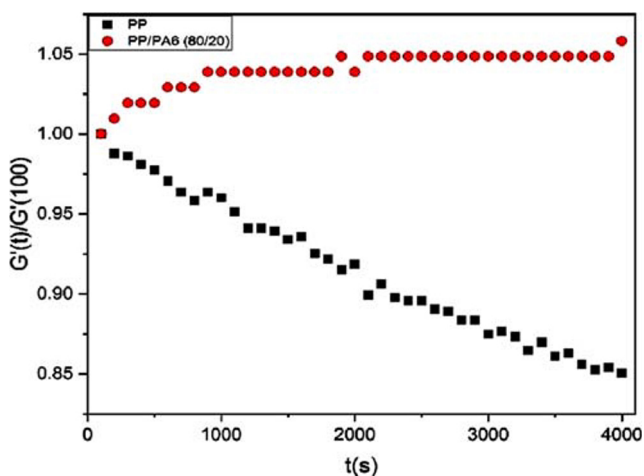
the investigated samples is equal, it can be concluded that the observed variation in rheological properties of the ternary blends is independent of the PA phase and it may originate from the morphological alteration during the time.

Shear-induced coarsening of the droplets at high temperatures is another undeniable effect in these systems. Figure 14 is plotted to show the distinct behavior of the blends as a function of frequency. An ascending trend at the low frequency zone is obvious for entire blends. Although shear-induced coalescence of the droplets in uncompatibilized polymeric blends generally stems from three steps (Allan and Mason 1962; Roland and Böuhm 1984; Sundararaj and Macosko 1995), in situ reaction at the surface of the droplets and matrix restricts this procedure to the second step and leads to a stabilized morphology by suppressing the coalescence (Sundararaj and Macosko 1995). However, at a higher temperature, compatibilized PA6 particles come close to each other owing to the lowered viscosity of the PP phase. As a result, in the blend containing 3.5 wt% of EPDM-g-MA, separated droplets rotate in the shear field and the intervening rubbery chains on the surface of them provide a rubbery field which can be seen as a tail in low frequencies.

An apparent point in this plot is the maximum instability observed in a blend containing 7.0 wt% rubbery phase. Another most important possibility for such variation in viscoelastic properties is the progress and completion of reactive compatibilization at elevated temperatures. This was tested using FTIR analysis applied for a blend sample that underwent the time sweep test at 230 and 270 °C (Fig. 15). The characteristic absorption peak of EPDM-g-MA presents at 1790 cm$^{-1}$ corresponding for anhydride-type carbonyls and 1710 cm$^{-1}$ to acid-type carbonyls. In the IR spectra of ternary blends (PP/PA6/EPDM-g-MA), the vanishing of the characteristic peak of EPDM-g-MA is a sign of perfect conversion of anhydride carbonyl groups to create EPDM-g-PA6 as a result of the reaction
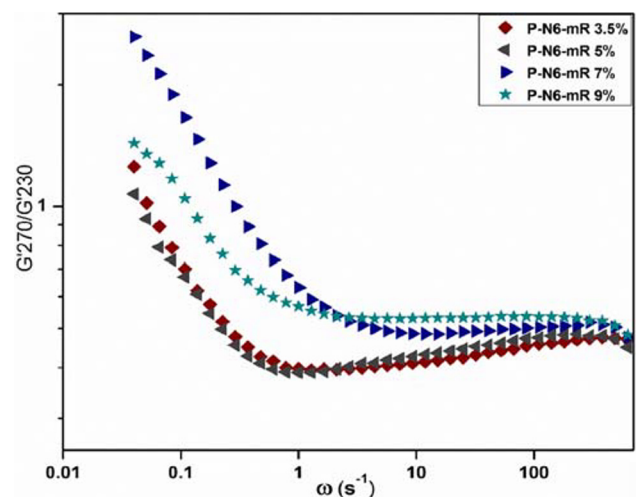


**Fig. 13** Time sweep test for iPP neat polymer and PP/PA6 (80/20) blend at 270 °C and 0.05 Hz
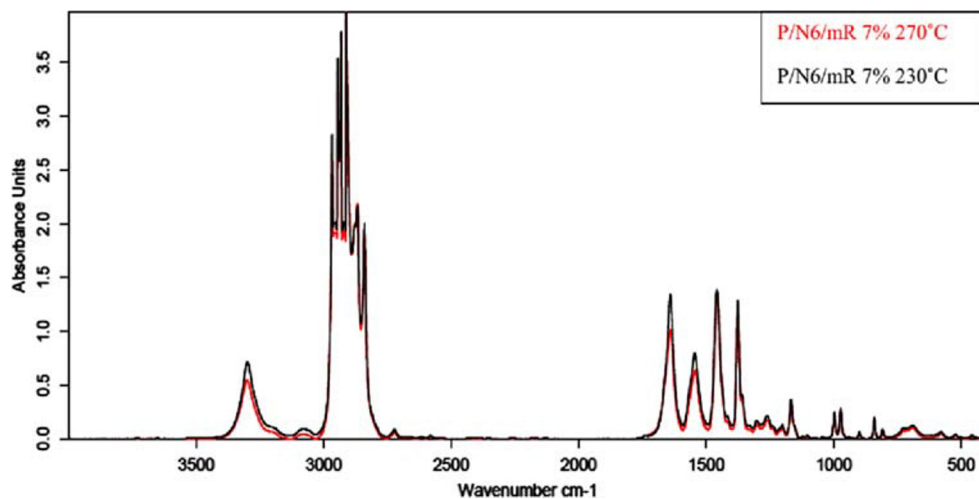


**Fig. 14** The ratio of the storage modulus at 270 °C to 230 °C (normalized storage modulus) vs. frequency for ternary blends with various EPDM-g-MA contents

**Fig. 15** FTIR spectra for PP/PA6/
EPDM-g-MA (80/20/7) at 230 °C
and 270 °C



between NH amide or $NH_2$ amine groups of PA6 with carbonyl groups of EPDM-g-MA at both temperatures (Malmir et al. 2012). Moreover, the intensities of the characteristic peaks for both the samples are almost the same. This shows that the in situ reactive compatibilization does not continue during the time sweep tests. Therefore, it can be claimed that the observed variation in the viscoelastic properties can only be due to the morphological alteration during the time sweep tests. To validate this assumption, the samples underwent the time sweep tests and were cryogenically fractured and morphologically analyzed. As

**Fig. 16** FESEM micrographs of morphology evolution in PP/PA6/EPDM-g-MA (80/20/7). **a** The quenched sample just after melt mixing. The samples underwent the time sweep tests at **b** 230 °C, **c** 250 °C, and **d** 270 °C for 4000 s
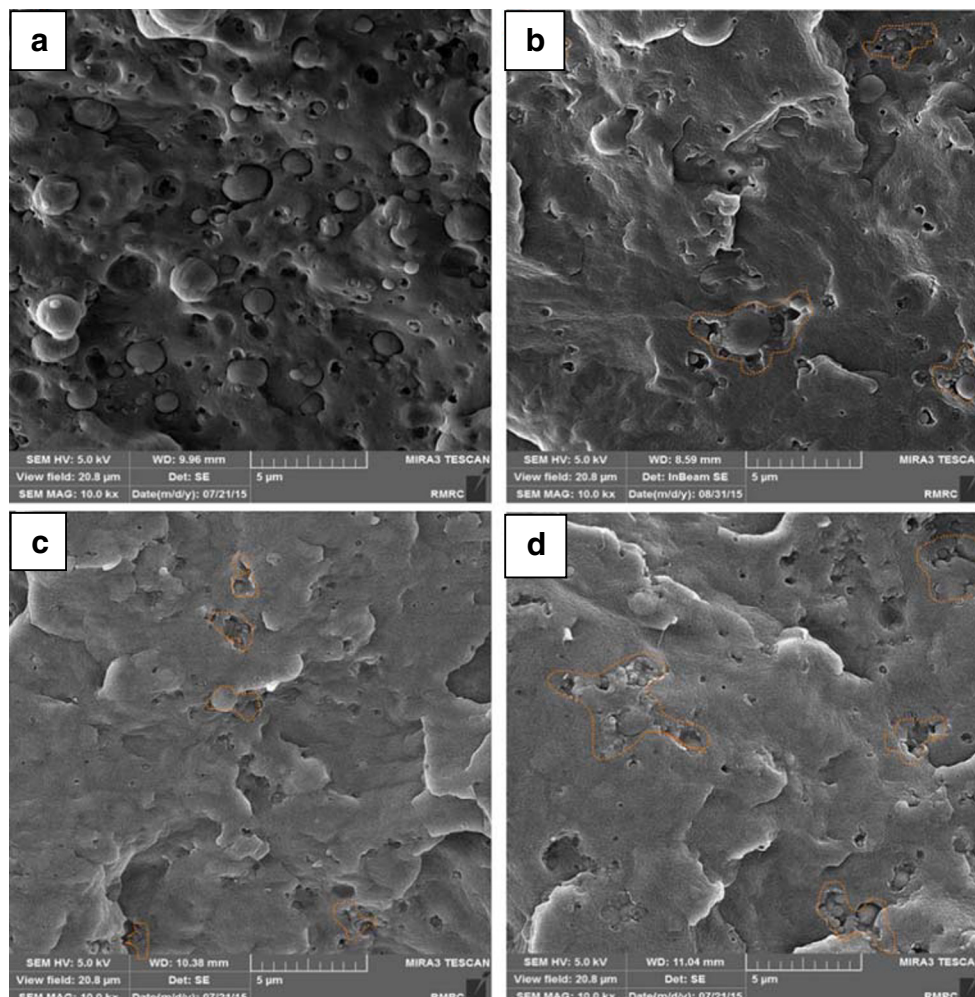
it can be observed in Fig. 16, this blend has an unstable morphology even at 230 °C annealing condition and also quenched condition, due to a higher amount of the rubbery phase. Therefore, it can be concluded that higher temperatures facilitate morphology instability and lead to aggregation of droplets, those covered by the rubber shell due to decreased viscosity of the matrix phase. Dotted areas in Fig. 16b–d show that the dimensions of the aggregated clusters increased by temperature.

## Conclusion

The rheology, morphology, and morphological stability of the reactive PP/PA6/EPDM-g-MA ternary blends at relatively low EPDM-g-MA contents as well as the reference binary blends were studied in detail, and the obtained results were conducted to the following conclusions:

The core-shell morphology was observed for reactive ternary blends confirming the predictions made by the theoretical analysis. The rubbery phase exhibited as an emulsification agent up to some extents above which the size of composite droplets increased due to the dominant effect of the viscosity ratio. This trend was also observed in the shape relaxation times of different compositions. It was also observed that the morphology of individual core-shell particles at low EPDM-g-MA contents transforms to the large clusters of these core-shell particles at higher rubbery phase contents along with the progressive increase in the shell thickness. This manifested itself in rheological properties by means that formation of aggregated clusters altered the viscoelastic behavior from liquid-like to solid-like. Alteration of the morphology was evaluated using time-sweep rheological experiments and confirmed via direct SEM analysis applied on the samples that underwent the time-sweep tests.

## References

Ajji A, Choplin L, Prud'Homme R (1988) Rheology and phase separation in polystyrene/poly (vinyl methyl ether) blends. J Polym Sci B Polym Phys 26(11):2279–2289

Allan R, Mason S (1962) Particle motions in sheared suspensions. XIV Coalescence of liquid drops in electric and shear fields. J Colloid Sci 17(4):383–408

Basseri G, Mehrabi Mazidi M, Hosseini F, Razavi Aghjeh MK (2014) Relationship among microstructure, linear viscoelastic behavior and mechanical properties of SBS triblock copolymer-compatibilized PP/SAN blend. Polym Bull 71(2):465–486

Codou A, Anstey A, Misra M, Mohanty AK (2018) Novel compatibilized nylon-based ternary blends with polypropylene and poly (lactic acid): morphology evolution and rheological behaviour. RSC Adv 8(28):15709–15724

Dealy J, Plazek D (2009) Time-temperature superposition—a user's guide. Rheol Bull 78(2):16–31

Díaz MF, Barbosa SE, Capiati NJ (2007) Reactive compatibilization of PE/PS blends. Effect of copolymer chain length on interfacial adhesion and mechanical behavior. Polymer 48(4):1058–1065

Dou R, Zhou Y, Shen C, Li LP, Yin B, Yang MB (2015) Toughening of PA6/EPDM-g-MAH/HDPE ternary blends via controlling EPDM-g-MAH grafting degree: the role of core–shell particle size and shell thickness. Polym Bull 72(2):177–193

Favis BD (1990) The effect of processing parameters on the morphology of an immiscible binary blend. J Appl Polym Sci 39(2):285–300

Graebling D, Muller R, Palierne J (1993a) Linear viscoelastic behavior of some incompatible polymer blends in the melt. Interpretation of data with a model of emulsion of viscoelastic liquids. Macromolecules 26(2):320–329

Graebling D., Muller R, and Palierne J (1993b) Linear viscoelasticity of incompatible polymer blends in the melt in relation with interfacial properties. Le Journal de Physique IV, 3(C7): p. C7–1525-C7–1534

Gramespacher H, Meissner J (1992) Interfacial tension between polymer melts measured by shear oscillations of their blends. J Rheol 36(6): 1127–1141

Guo H et al (1997a) Prediction and manipulation of the phase morphologies of multiphase polymer blends: 1. Ternary systems. Polymer 38(4):785–794

Guo H-F, Gvozdic N, Meier D (1997b) Prediction and manipulation of the phase morphologies of multiphase polymer blends: II. Quaternary systems. Polymer 38(19):4915–4923

Han C (1981) Multiphase flow in polymer processing academic. New York: p:81–147

Hasanpour M, Aghjeh MR, Mazidi MM, Afsari B (2019) Effect of morphology alteration on mechanical properties and fracture toughness of polypropylene/polyamide 6/ethylene polypropylene diene monomer graft maleic anhydride (PP/PA6/EPDM-g-MA) reactive ternary blends. Polym Bull:1–28

Hemmati M, Nazokdast H, Shariat Panahi H (2001a) Study on morphology of ternary polymer blends. I Effects of melt viscosity and interfacial interaction. J Appl Polym Sci 82(5):1129–1137

Hemmati M, Nazokdast H, Shariat Panahi H (2001b) Study on morphology of ternary polymer blends. II Effect of composition. J Appl Polym Sci 82(5):1138–1146

Hobbs S, Dekkers M, Watkins V (1988) Effect of interfacial forces on polymer blend morphologies. Polymer 29(9):1598–1602

Horiuchi S, Nakayama K (1999) Morphology development during melt processing of immiscible polymer blends, macromolecular science and engineering. Springer p 301-318

Horiuchi S, Matchariyakul N, Yase K, Kitano T (1997) Morphology development through an interfacial reaction in ternary immiscible polymer blends. Macromolecules 30(12):3664–3670

Jacobs U, Fahrländer M, Winterhalter J, Friedrich C (1999) Analysis of Palierne's emulsion model in the case of viscoelastic interfacial properties. J Rheol 43(6):1495–1509

Jazani OM, Arefazar A, Jafari SH, Beheshty MH, Ghaemi A (2011) A study on the effects of SEBS-g-MAH on the phase morphology and mechanical properties of polypropylene/polycarbonate/SEBS ternary polymer blends. J Appl Polym Sci 121(5):2680–2687

Jazani OM, Arefazar A, Jafari SH, Peymanfar MR, Saeb MR, Talaei A (2013) SEBS-g-MAH as a reactive compatibilizer precursor for PP/PTT/SEBS ternary blends: morphology and mechanical properties. Polym-Plast Technol Eng 52(2):206–212

Khanna Y, Han P, Day E (1996) New developments in the melt rheology of nylons. I: effect of moisture and molecular weight. Polym Eng Sci 36(13):1745–1754

Kim TY, Kim DM, Kim WJ, Lee TH, Suh KS (2004) Effects of poly [styrene-b-(ethylene-co-butylene) -b-styrene] on the charge distributions of low-density polyethylene/polystyrene blends. J Polym Sci B Polym Phys 42(15):2813–2820

Krache R, Benachour D, Pötschke P (2004) Binary and ternary blends of polyethylene, polypropylene, and polyamide 6, 6: the effect of

compatibilization on the morphology and rheology. J Appl Polym Sci 94(5):1976–1985

Laun H (1979) Viscoelastic behavior of polyamide-6 melts. Rheol Acta 18(4):478–491

Lee HG, Sung YT, Lee YK, Kim WN, Yoon HG, Lee HS (2009) Effects of PP-g-MAH on the mechanical, morphological and rheological properties of polypropylene and poly (acrylonitrile-butadiene-styrene) blends. Macromol Res 17(6):417–423

Li L-p et al (2012) Characterization of PA6/EPDM-g-MA/HDPE ternary blends: the role of core-shell structure. Polymer 53(14):3043–3051

Li R, Yu W, Zhou C (2006) Rheological characterization of droplet-matrix versus co-continuous morphology. J Macromol Sci Part B 45(5):889–898

Li X, Pozrikidis C (1997) The effect of surfactants on drop deformation and on the rheology of dilute emulsions in stokes flow. J Fluid Mech 341:165–194

Liu C, He J, Van Ruymbeke E, Keunings R, Bailly C (2006) Evaluation of different methods for the determination of the plateau modulus and the entanglement molecular weight. Polymer 47(13):4461–4479

López-Barrón CR, Macosko CW (2012) Rheological and morphological study of cocontinuous polymer blends during coarsening. J Rheol 56(6):1315–1334

Malmir S et al (2012) Relationship between morphology and rheology of PA/PE/clay blend nanocomposites. I. PA matrix. J Appl Polym Sci 125(S1)

Marin G, Labaig J, Monge P (1975) Dynamic viscoelasticity of entangled polymers. Polymer 16(3):223–226

Martin P, Carreau PJ, Favis BD, Jérôme R (2000) Investigating the morphology/rheology interrelationships in immiscible polymer blends. J Rheol 44(3):569–583

Mazidi MM, Aghjeh MKR (2015) Effects of blend composition and compatibilization on the melt rheology and phase morphology of binary and ternary PP/PA6/EPDM blends. Polym Bull 72(8):1975–2000

Mazidi MM, Razavi Aghjeh MK, Khonakdar HA, Reuter U (2016) Structure–property relationships in super-toughened polypropylene-based ternary blends of core–shell morphology. RSC Adv 6(2):1508–1526

Mazzeo FA (2012) Importance of oscillatory time sweeps in rheology. TA Instruments: p 1–4

Ninomiya K, Ferry JD (1959) Some approximate equations useful in the phenomenological treatment of linear viscoelastic data. J Colloid Sci 14(1):36–48

Omonov TS, Harrats C, Groeninckx G (2005) Co-continuous and encapsulated three phase morphologies in uncompatibilized and reactively compatibilized polyamide 6/polypropylene/polystyrene ternary blends using two reactive precursors. Polymer 46(26):12322–12336

Palierne J (1990) Linear rheology of viscoelastic emulsions with interfacial tension. Rheol Acta 29(3):204–214

Paul, D.R. (2012) Polymer blends. Vol. 1: Elsevier

Pawar Y, Stebe KJ (1996) Marangoni effects on drop deformation in an extensional flow: the role of surfactant physical chemistry. I Insoluble surfactants. Phys Fluids 8(7):1738–1751

Purnima D, Maiti S, Gupta A (2006) Interfacial adhesion through maleic anhydride grafting of EPDM in PP/EPDM blend. J Appl Polym Sci 102(6):5528–5532

Rastin H, Jafari SH, Saeb MR, Khonakdar HA, Wagenknecht U, Heinrich G (2014) On the reliability of existing theoretical models in anticipating type of morphology and domain size in HDPE/PA-6/EVOH ternary blends. Eur Polym J 53:1–12

Ravati S, Favis BD (2010) Morphological states for a ternary polymer blend demonstrating complete wetting. Polymer 51(20):4547–4561

Reignier J, Favis BD (2000) Control of the subinclusion microstructure in HDPE/PS/PMMA ternary blends. Macromolecules 33(19):6998–7008

Reignier J, Favis BD (2003) Core–shell structure and segregation effects in composite droplet polymer blends. AICHE J 49(4):1014–1023

Reignier J, Favis BD, Heuzey MC (2003) Factors influencing encapsulation behavior in composite droplet-type polymer blends. Polymer 44(1):49–59

Riemann R-E, Cantow H-J, Friedrich C (1996) Rheological investigation of form relaxation and interface relaxation processes in polymer blends. Polym Bull 36(5):637–643

Riemann R-E, Cantow H-J, Friedrich C (1997) Interpretation of a new interface-governed relaxation process in compatibilized polymer blends. Macromolecules 30(18):5476–5484

Roland C, Böuhm G (1984) Shear-induced coalescence in two-phase polymeric systems. I Determination from small-angle neutron scattering measurements. J Polym Sci Polym Phys Ed 22(1):79–93

Sailer CF (2008) Blends of polyamide 6 and Styrenic polymers: influence of reactive compatibilization on melt rheology and morpholog, ETH

Salehiyan R, Ray SS (2018) Processing of polymer blends, emphasizing: melt compounding; influence of nanoparticles on blend morphology and rheology; reactive processing in ternary systems; morphology–property relationships; performance and application challenges; and opportunities and future trends, In processing of polymer-based Nanocomposites (pp. 167–197). Springer, Cham

Seo YP, Seo Y (2018) Effect of molecular structure change on the melt rheological properties of a polyamide (nylon 6). ACS omega 3(12):16549–16555

Shi D, Ke Z, Yang J, Gao Y, Wu J, Yin J (2002) Rheology and morphology of reactively compatibilized PP/PA6 blends. Macromolecules 35(21):8005–8012

Shi D, Hu GH, Ke Z, Li RKY, Yin J (2006) Relaxation behavior of polymer blends with complex morphologies: Palierne emulsion model for uncompatibilized and compatibilized PP/PA6 blends. Polymer 47(13):4659–4666

Shokoohi S, Arefazar A, Naderi G (2012) Compatibilized PP/EPDM/PA6 ternary blends: extended morphological studies. Polym Adv Technol 23(3):418–424

Silva J, Machado AV, Moldenaers P, Maia J (2010) The effect of interfacial properties on the deformation and relaxation behavior of PMMA/PS blends. J Rheol 54(4):797–813

Stone H, Leal L (1990) The effects of surfactants on drop deformation and breakup. J Fluid Mech 220:161–186

Sundararaj U, Macosko C (1995) Drop breakup and coalescence in polymer blends: the effects of concentration and compatibilization. Macromolecules 28(8):2647–2657

Tchomakov KP et al (2004) Composite droplets with core/shell morphologies prepared from HDPE/PS/PMMA ternary blends by twin-screw extrusion. Polym Eng Sci 44(4):749

Utracki LA, Wilkie CA (2002) Polymer blends handbook (Vol. 1, p. 2). Kluwer academic publishers, Dordrecht

Valera TS, Morita AT, Demarquette NR (2006) Study of morphologies of PMMA/PP/PS ternary blends. Macromolecules 39(7):2663–2675

Van Gurp M, Palmen J (1998) Time-temperature superposition for polymeric blends. Rheol Bull 67(1):5–8

Van Puyvelde P, Velankar S, Moldenaers P (2001) Rheology and morphology of compatibilized polymer blends. Curr Opin Colloid Interface Sci 6(5):457–463

Vanoene H (1972) Modes of dispersion of viscoelastic fluids in flow. J Colloid Interface Sci 40(3):448–467

Velankar S, van Puyvelde P, Mewis J, Moldenaers P (2001) Effect of compatibilization on the breakup of polymeric drops in shear flow. J Rheol 45(4):1007–1019

Vinckier I, Moldenaers P, Mewis J (1996) Relationship between rheology and morphology of model blends in steady shear flow. J Rheol 40(4):613–631

Wang D, Xie X-M (2006) Novel strategy for ternary polymer blend compatibilization. Polymer 47(23):7859–7863

Wang D, Li Y, Xie XM, Guo BH (2011) Compatibilization and morphology development of immiscible ternary polymer blends. Polymer 52(1):191–200

Wilkinson A et al (1999) Phase structure in polypropylene/PA6/SEBS blends. Polymer 40(17):4971–4975

Wilkinson A, Clemens M, Harding V (2004) The effects of SEBS-g-maleic anhydride reaction on the morphology and properties of polypropylene/PA6/SEBS ternary blends. Polymer, 2004 45(15): 5239–5249

Wu S (1987) Formation of dispersed phase in incompatible polymer blends: interfacial and rheological effects. Polym Eng Sci 27(5): 335–343

Yin B, Zhao Y, Yu RZ, An HN, Yang MB (2007) Morphology development of PC/PE blends during compounding in a twin-screw extruder. Polym Eng Sci 47(1):14–25

Yin B, Li LP, Zhou Y, Gong L, Yang MB, Xie BH (2013) Largely improved impact toughness of PA6/EPDM-g-MA/HDPE ternary blends: the role of core–shell particles formed in melt processing on preventing micro-crack propagation. Polymer 54(7):1938–1947

Zhang J, Ravati S, Virgilio N, Favis BD (2007) Ultralow percolation thresholds in ternary cocontinuous polymer blends. Macromolecules 40(25):8817–8820

Zhou Y, Wang W, Dou R, Li LP, Yin B, Yang MB (2013) Effect of EPDM-g-MAH on the morphology and properties of PA6/EPDM/HDPE ternary blends. Polym Eng Sci 53(9):1845–1855